Modelling the flux distribution function of the extragalactic γ-ray background from dark matter annihilation

Feyereisen, Ando, and Lee

JCAP09 (2015) 027

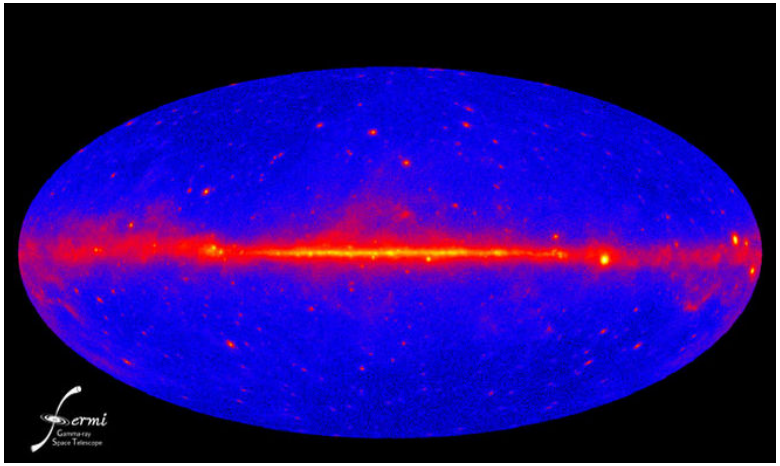

→ The one-point function (i.e., the isotropic flux distribution) is a complementary method to (anisotropic) two-point correlations in searches for a gamma-ray dark matter annihilation signature.

→ Using analytical models of structure formation and dark matter halo properties, we compute the gamma-ray flux distribution due to annihilations in extragalactic dark matter halos, as it would be observed by the Fermi Large Area Telescope.

→ We show that by using the flux distribution at only one energy bin, one can probe the canonical cross-section required for explaining the relic density, for dark matter of masses around tens of GeV.

2.1 PDF for the flux from individual halos

Throughout the paper, F represents the *differential* flux, i.e., a number of photons received per unit area, unit time, and unit energy range [$F(E) = d^3N_\gamma/dAdtdE$]. The PDF $P(F)$ for observing a total differential flux F from all of the halos in a pixel depends on the PDF $P_1(F)$ for observing F from any individual halo.[1] We thus proceed by first deriving the latter quantity.

Because the differential flux F from an individual halo is completely determined by its rest-frame differential luminosity $L = d^2N_\gamma/dtdE$ and its redshift z, we can write

$$P_1(F) = \int dL\, dz\, P(F|L,z)P(L,z)$$
$$= \int dL\, dz\, \delta[F - F(L,z)]P(L|z)P(z) \tag{2.1}$$

Here, the usual relation for the differential flux,

$$F(E;L,z) = e^{-\tau(E,z)}\frac{(1+z)^2 L[(1+z)E]}{4\pi d_L^2(z)}\,, \tag{2.2}$$

[1] Throughout this paper, we denote probability distributions by $P(\cdots)$ and distinguish them using the random variables that they describe, along with subscripts if necessary. Conditional and parameterised distributions are denoted as $P(\cdot|\cdot)$. Exceptions to this convention are Poisson and Normal distributions, denoted $\mathcal{P}(\cdot|\cdot)$ and $\mathcal{G}(\cdot|\cdot,\cdot)$ respectively.

X has probability density function g

$$\mathbb{P}(E) = \sum_{x\in S} g(x)\mathbb{P}(E \mid X = x)$$
$$\mathbb{P}(E) = \int_S g(x)\mathbb{P}(E \mid X = x)\,dx$$

(X,Y) has joint probability density function f.

$$g(x) = \sum_{y\in T} f(x,y), \quad x \in S$$
$$g(x) = \int_T f(x,y)\,dx \quad x \in S$$
$$h(y \mid x) = \frac{f(x,y)}{g(x)}$$

[you can then check that]

$$\int_T h(y \mid x)\,dy = 1$$
$$\mathbb{P}(Y \in B \mid X = x) = \int_B h(y \mid x)\,dy$$

PDF of observing $P_1(F)$ from any individual halo

$$P_1(F) = \int dL\, dz\, \delta[F - F(L,z)] P(L|z) P(z)$$

We can interpret $P(L|z) = dN/dL(z)$ as the redshift-dependent halo differential-luminosity function.[2] Assuming that the halos are isotropically distributed across the Universe, the number of halos at redshift z is proportional to the comoving volume $\delta V(z)$ of the corresponding redshift slice δz, therefore we also have $P(z) = dN/dz \propto dV/dz$.

Alternatively, we can rewrite eq. (2.1) in terms of the halo mass M to obtain

$$P_1(F) = \int dL\, dM\, dz\, \delta[F - F(L,z)] P(L|M,z) P(M|z) P(z)\,,$$

where we can similarly interpret $P(M|z) = dN/dM(z)$ as the redshift-dependent halo mass

the halo, which usually shows scatter for any given M. The halo profiles can be completely characterised by some parameters $\boldsymbol{\theta}_{\rm h}$ (such as $\rho_{\rm s}, r_{\rm s}, r_{\rm vir} \ldots$ in the case of the NFW profile [29]) so that (for any given particle dark matter model) we have $L = L(\boldsymbol{\theta}_{\rm h})$. If we further assume that the distribution of halo profiles can be described by a halo model that gives $P(\boldsymbol{\theta}_{\rm h}|M,z)$, we can write

$$P(L|M,z) = \int d\boldsymbol{\theta}_{\rm h}\, P(L|\boldsymbol{\theta}_{\rm h}) P(\boldsymbol{\theta}_{\rm h}|M,z) = \int d\boldsymbol{\theta}_{\rm h}\, \delta[L - L(\boldsymbol{\theta}_{\rm h})] P(\boldsymbol{\theta}_{\rm h}|M,z)$$

$$P_1(F) = \int dM\, dz\, d\boldsymbol{\theta}_{\rm h}\, \delta[F - F(\boldsymbol{\theta}_{\rm h},z)] P(\boldsymbol{\theta}_{\rm h}|M,z) P(M|z) P(z)\,,$$

PDF of observing $P_1(F)$ from any individual halo (in a pixel)

$$P_1(F) = \int dM\, dz\, d\boldsymbol{\theta}_\mathrm{h}\, \delta[F - F(\boldsymbol{\theta}_\mathrm{h}, z)] P(\boldsymbol{\theta}_\mathrm{h}|M, z) P(M|z) P(z)$$

$$P(M|z) = dN/dM(z)$$

$$P(z) = dN/dz \propto dV/dz.$$

In order to make the numerical calculation of eq. (2.5) more tractable, we shall neglect the scatter in the distribution $P(\boldsymbol{\theta}_\mathrm{h}|M, z)$ in this work. That is, we take the distribution of the halo-profile parameters $\boldsymbol{\theta}_\mathrm{h} = \{\theta_{\mathrm{h},1}, \ldots, \theta_{\mathrm{h},n}\}$ to be given by

$$P(\boldsymbol{\theta}_\mathrm{h}|M, z) = \prod_{i=1}^{n} \delta[\theta_{\mathrm{h},i} - \bar{\theta}_{\mathrm{h},i}(M, z)]\,, \tag{2.6}$$

where the functions $\bar{\theta}_{\mathrm{h},i}(M, z)$ give the mean values for the parameters. With this assumption, we can perform the integrals over $\boldsymbol{\theta}_\mathrm{h}$ and M in eq. (2.5), leaving only an integral over z:

$$P_1(F) = \int dz \left|\frac{\partial F}{\partial M}\right|^{-1} \frac{dN}{dM}\frac{dV}{dz}\,. \tag{2.7}$$

To find the probability function in a set of transformed variables, find the Jacobian. For example, If $u = u(x)$, then

$P_u\, du = P_x\, dx$,

so

$P_u = P_x \left|\frac{\partial x}{\partial u}\right|$.

PDF of observing $P_1(F)$ and $P(F)$ [single vs all halos in pixel]

$$P_1(F) = \int dz \left|\frac{\partial F}{\partial M}\right|^{-1} \frac{dN}{dM}\frac{dV}{dz}\,.$$

We assume that all dark matter gamma-ray sources may be treated as point sources (see also section 3.1.1 and section 5.4 below), allowing us to equate the differential flux F and the differential flux per pixel. The dark matter differential flux F arriving at any given pixel of the Fermi sky map, is the summed flux $F = \sum_i F_i$ of any number of individual halo point sources [30], where each differential flux F_i is an independent and identically distributed (i.i.d.) random variable with the distribution $P_1(F)$. The distribution of a sum of random variables is the convolution of all the original distributions [31]; since the F_i are i.i.d., the distribution of the total differential flux per pixel is the autoconvolution [25]

$$P_k(F) = P_1(F) \star P_1(F) \star \cdots \star P_1(F) = (P_1)^{\star k}\,, \tag{2.8}$$

where k is the number of halos contributing to this flux. Since furthermore we do not know how many halos are thus stacked in a pixel, the number k of fluxes in the sum is itself a random variable. If we assume this number k of halos per pixel is Poisson-distributed over the sky with some mean N', we can model the *total* differential flux per pixel as

$$P(F) = \int dN' P(N') \sum_k \mathcal{P}\left(k|N'\right) P_k(F)\,, \tag{2.9}$$

where the uncertainties in k and N' are marginalised away. Since the numbers k and N' of extragalactic halos are very large, both $P(N')$ and $\mathcal{P}\left(k|N'\right)$ are thin enough to be approximated by delta functions, so that $P(F) = P_{k\approx N'}(F)$. Thus, the only additional physical input required to compute $P(F)$ from $P_1(F)$ is N', which is discussed below.

PDF of observing $P_1(F)$ and $P(F)$ [single vs all halos in pixel]

$$P_1(F) = \int dz \left|\frac{\partial F}{\partial M}\right|^{-1} \frac{dN}{dM}\frac{dV}{dz}\,.$$

$$P_k(F) = P_1(F) \star P_1(F) \star \cdots \star P_1(F) = (P_1)^{\star k}$$

$$P(F) = P_{k\approx N'}(F).$$

3.1.1 Number of halos per Fermi pixel

Cosmology directly determines the redshift distribution of halos (via isotropy $P(z) = dN/dz$) and their mass distribution (via the gravitational collapse of inhomogeneities that yields dN/dM). The normalisation of these number densities clearly corresponds to the total number N of halos in the Universe. The number of halos per Fermi pixel is then

$$N' = \frac{\Omega_{\rm pix}}{4\pi} N = \frac{\Omega_{\rm pix}}{4\pi} \int \frac{dN}{dM}\frac{dV}{dz} dM dz\,, \qquad (3.1)$$

PSF(Fermi-Lat)~0.8° → N'~ 7 10^{21}

PDF of observing $P_1(F)$ and $P(F)$ [single vs all halos in pixel]

$$P_1(F) = \int dz \left|\frac{\partial F}{\partial M}\right|^{-1} \frac{dN}{dM}\frac{dV}{dz}.$$

$$P_k(F) = P_1(F) \star P_1(F) \star \cdots \star P_1(F) = (P_1)^{\star k}$$

$$P(F) = P_{k \approx N'}(F).$$

3.1.2 Halo mass function

The halo mass function, first addressed heuristically by Press and Schechter [38] and subsequently formalised in, e.g., ref. [39], is computed as

$$\frac{dn}{dM} = \frac{\bar{\rho}}{M} f(\nu) \frac{d\nu}{dM}, \qquad \nu = \left(\frac{\delta_c}{\sigma}\right)^2, \tag{3.4}$$

where $\delta_c = 1.69/D(z)$ is the (linear) critical overdensity, $D(z)$ is the linear growth factor, and $\sigma(M)$ is the rms deviation of primordial density fluctuations, smoothed to scale M [39]. The functional form of $\sigma(M)$ (required to calculate $d\nu/dM$) is determined from the literature [40] with normalisation set by the cosmological parameter σ_8 [32]. The function $f(\nu)$ is derived from the excursions of these density fluctuations above a 'barrier' [39] that encodes the physics of halo collapse (including δ_c). For an approachable presentation of the formalism, see ref. [41].

In addition to ellipsoidal collapse, our fiducial mass function incorporates a virialised halo's angular momentum and the cosmological constant into its barrier δ_c. It has a self-similar $f(\nu)$ well-fit by the following function (eq. (163) in [42, 43]):

$$\nu f(\nu) \propto \left(1 + \frac{0.1218}{(a\nu)^{0.585}} + \frac{0.0079}{(a\nu)^{0.4}}\right) \sqrt{\frac{a\nu}{2\pi}} \exp\left(-0.4019 a\nu \left[1 + \frac{0.5526}{(a\nu)^{0.585}} + \frac{0.02}{(a\nu)^{0.4}}\right]^2\right),$$

PDF of observing $P_1(F)$ and $P(F)$ [single vs all halos in pixel]

$$P_1(F) = \int dz \left|\frac{\partial F}{\partial M}\right|^{-1} \frac{dN}{dM}\frac{dV}{dz}.$$

$$P_k(F) = P_1(F) \star P_1(F) \star \cdots \star P_1(F) = (P_1)^{\star k}$$

$$P(F) = P_{k\approx N'}(F).$$

3.2 Halo model

The differential luminosity from annihilation in a dark matter halo of mass M is given by the product of a particle physics term and an astrophysical J-factor, i.e. the line-of-sight integral of the dark matter density squared, boosted by the annihilations in halo substructures. The dark matter density can be parameterised using the same profiles that fit N-body simulations well. For an NFW profile, the J factor of a point-like source can be analytically recast as

$$J = (1 + B)\, a(c_{\rm vir})\rho_{\rm s} M_{\rm vir}, \tag{3.5}$$

in terms of the substructure boost B, the virial concentration $c_{\rm vir}$, the scale density $\rho_{\rm s}$ of the profile, and the analytic function (e.g., [46])

$$a(c) = \left(1 - \frac{1}{(1+c)^3}\right)\left(\ln(1+c) - \frac{c}{1+c}\right)^{-2}.$$

PDF of observing $P_1(F)$ and $P(F)$ [single vs all halos in pixel]

$$P_1(F) = \int dz \left|\frac{\partial F}{\partial M}\right|^{-1} \frac{dN}{dM}\frac{dV}{dz}\,.$$

$$P_k(F) = P_1(F) \star P_1(F) \star \cdots \star P_1(F) = (P_1)^{\star k}$$

$$P(F) = P_{k\approx N'}(F).$$

3.3 The gamma-ray model

3.3.1 Dark matter annihilation model

The particle physics component $K(E) = \langle\sigma v\rangle(dN/dE)/m_\chi^2$ of this model ($L(E) = JK(E)$) is assumed here to be a standard WIMP model, with annihilations into gamma rays via $b\bar{b}$. $\langle\sigma v\rangle$ is taken to be the thermal cross-section $3\times10^{-26}\,\mathrm{cm}^3\,\mathrm{s}^{-1}$, and the WIMP mass is taken to be $m_\chi = 85\,\mathrm{GeV}$. Our parameterisation of the photon number per energy per annihilating particle is [53]:

$$\frac{dN}{dE} = \frac{0.42\exp(-8x)}{m_\chi(x^{1.5}+0.00014)}, \qquad x = \frac{E}{m_\chi}\,. \tag{3.8}$$

3.3.2 Gamma-ray optical depth

By restricting our analysis to small enough redshifts and energies, we do not need to consider photoionisation or pair production [54]. We can then use a very rough parameterisation [53] of gamma-ray absorbtion:

$$e^{-\tau(E,z)} = \exp\left[-\frac{z}{3.3}\left(\frac{E}{10\mathrm{GeV}}\right)^{0.8}\right]. \tag{3.9}$$

PDF of observing $P_1(F)$ from any individual halo (in a pixel)

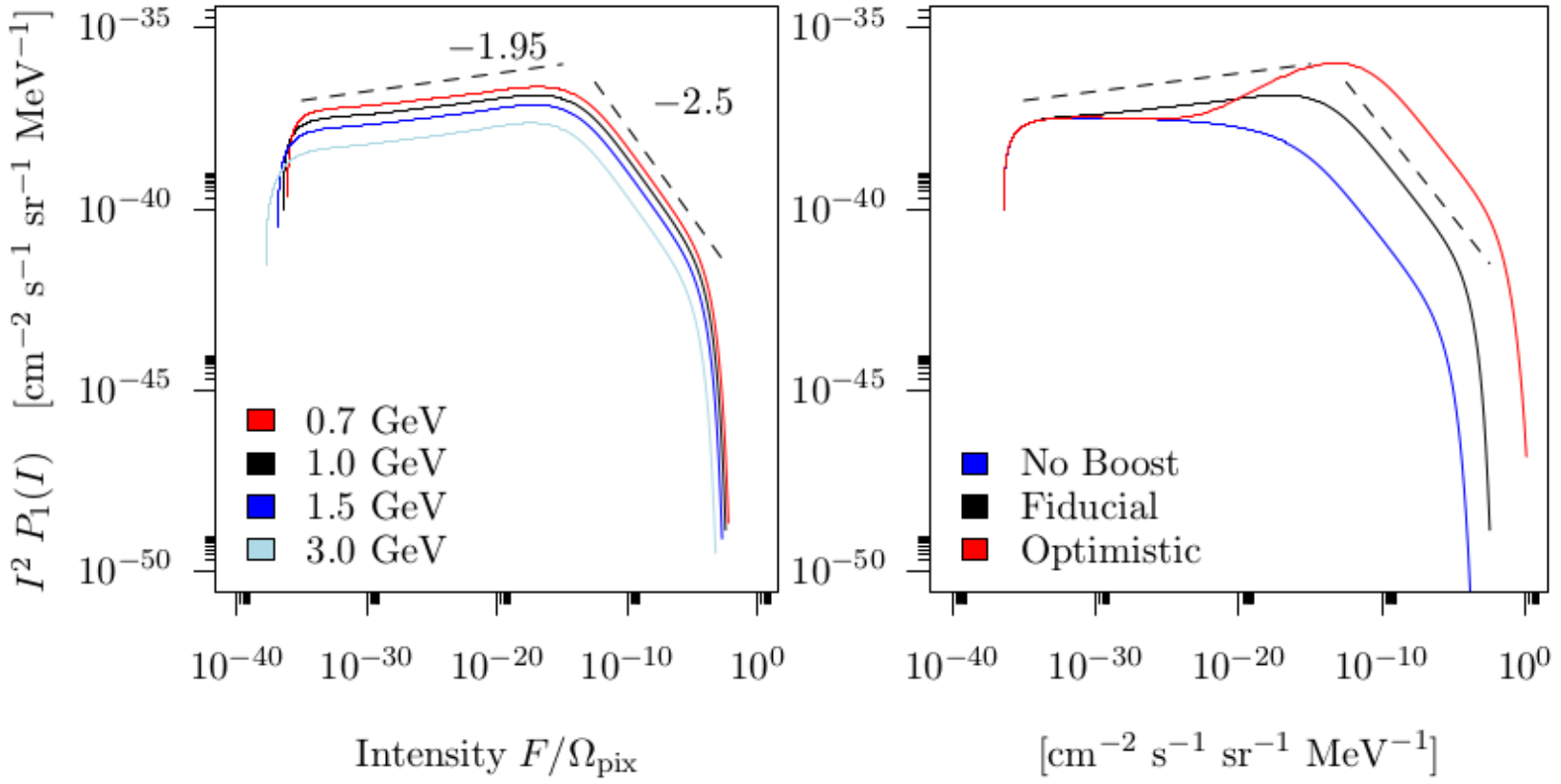

Figure 1. The flux/intensity PDF for a single dark matter source, $P_1(F)$, with its dependence on photon energy (left) and boost models (right). In the right panel, the blue, black, and red curves represent respectively the pessimistic, fiducial, and optimistic models of the subhalo boost. The choice of boost model clearly and significantly affects the functional form of the one-point function. The log-slopes of the fiducial model are offset (black dashed) and quantified for convenience. The flux F and intensity I of the gamma-ray background are related via the instrument's pixel size: $F = I\Omega_{\rm pix}$, where $\Omega_{\rm pix} \approx 5.8 \times 10^{-4}$ sr for $E = 1\,\mathrm{GeV}$ photons.

PDF of observing $P_1(F)$ from any individual halo (in a pixel)

We will need, when computing the total $P(F)$, to compute the first few moments of $P_1(F)$ at an intermediate step:

$$\mathbb{E}_{P_1(F)} = \int dF' P_1(F') F' \,, \tag{4.1}$$

$$\mathbb{V}_{P_1(F)} = \int dF' P_1(F') (F' - \mathbb{E}_{P_1(F)})^2 \,. \tag{4.2}$$

After multiplying eq. (4.1) by the mean number of halos [eq. (3.1)] and dividing by the pixel size, one obtains the mean intensity of the gamma-ray background from dark matter annihilation [61]. Similarly the variance [eq. (4.2)] is related to the angular power spectrum after similar corrections [62].

Since eq. (2.7) entails an integration over redshift for each F, and since we find $P_1(F)$ to be relatively smooth, we calculate 250 logarithmically equidistant points over the ∼40 orders of magnitude supporting the distribution. In order to obtain robust estimate of the moments, we further sample 250 points within the four orders of magnitude nearest to the maximum estimated from the low-resolution sampling.

PDF of observing $P_1(F)$ from any individual halo (in a pixel)

$$\mathbb{E}_{P_1(F)} = \int dF' P_1(F') F' \,, \tag{4.1}$$

$$\mathbb{V}_{P_1(F)} = \int dF' P_1(F') (F' - \mathbb{E}_{P_1(F)})^2 \,. \tag{4.2}$$

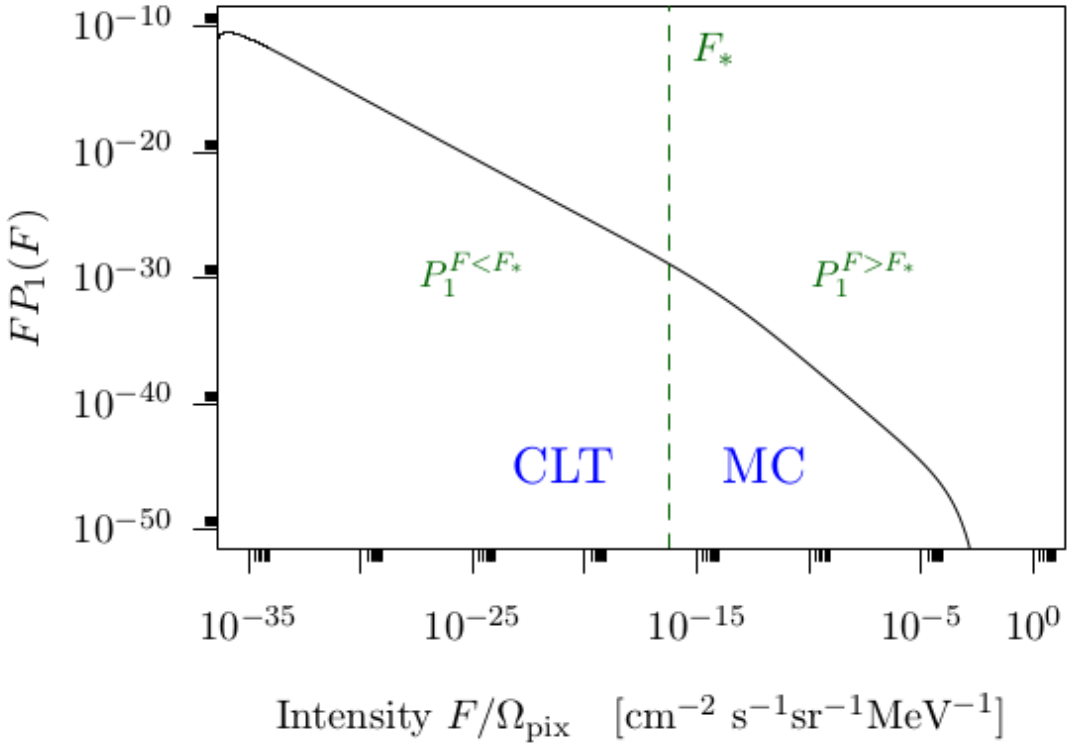

Figure 2. Schematic of the F_* cutoff of $P_1(F)$ into high/low flux. In our computation of the full $P(F)$, the central limit theorem is used to combine the fluxes from the many sources fainter than F_*, that follow a distribution $P_1^{F<F_*}(F)$. Monte Carlo is used above this cutoff to combine the halo fluxes drawn from $P_1^{F>F_*}(F)$.

PDF of observing P(F) [all halos in pixel]: DM extragalactic

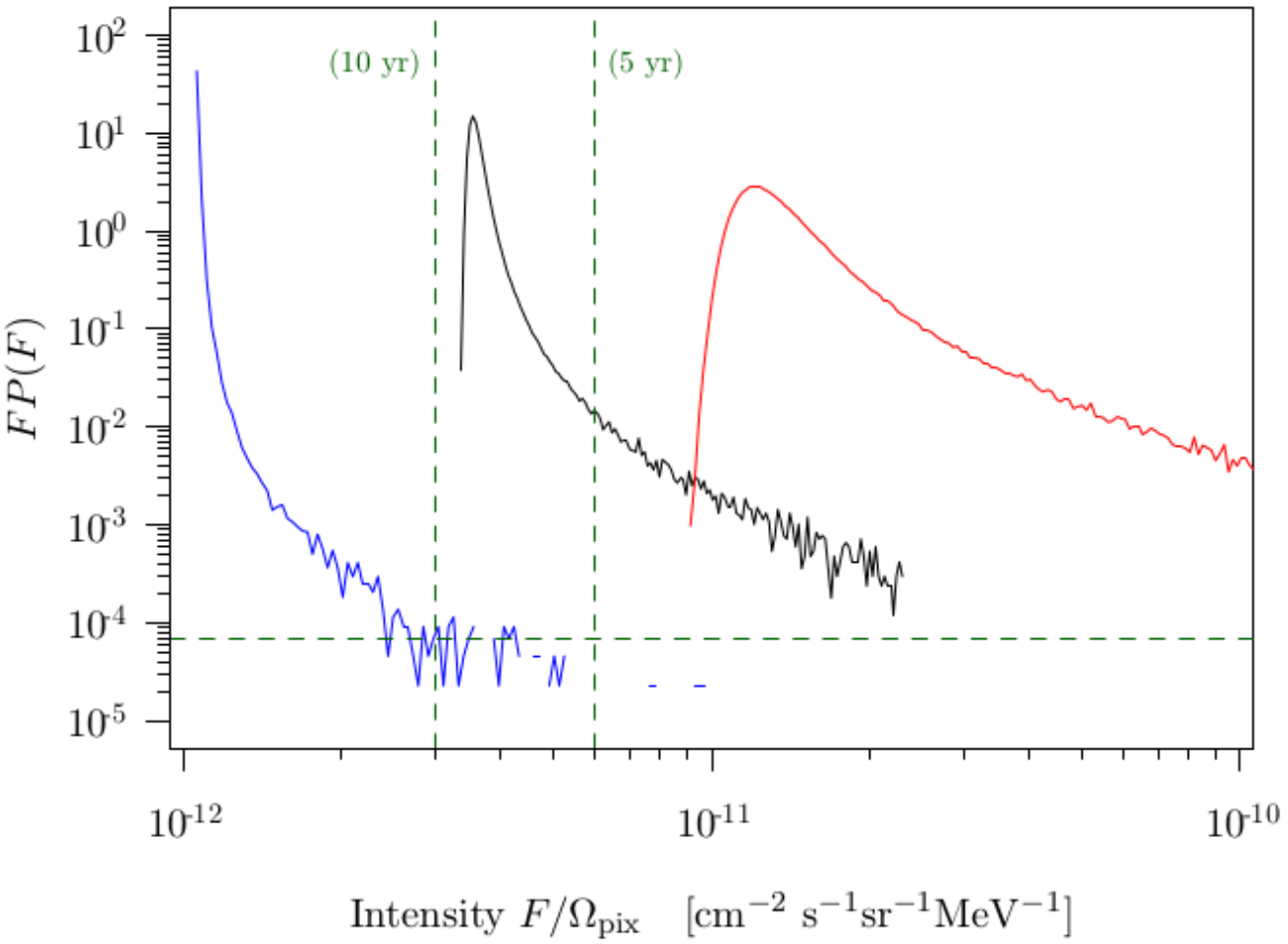

Figure 3. The flux PDF $P(F)$ per pixel. The blue, black, and red curves represent respectively the pessimistic, fiducial, and optimistic models of the subhalo boost. Instrumental responses of Fermi-LAT on detecting $P(F)$ are schematically shown. Vertical lines represent a flux corresponding to a single, one GeV photon per pixel, over the course of a mission of duration 5 (10) years. The Horizontal line schematises the angular resolution limit [eq. (4.4)] at 1 GeV.

PDF of observing P(F) [all halos in pixel]: DM extragalactic vs dSphs

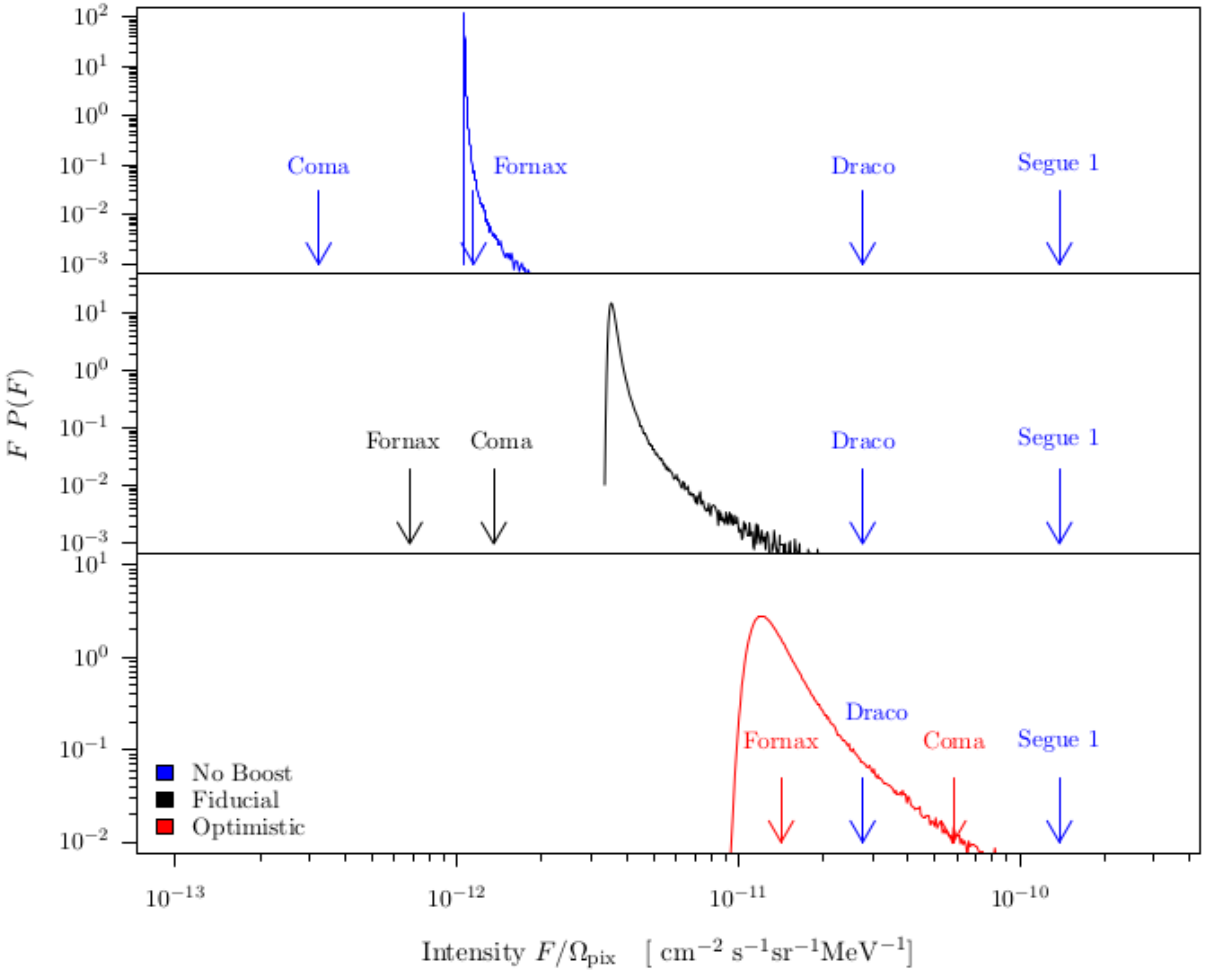

Figure 4. Brightnesses of promising clusters and dwarf spheroidal galaxies superposed on the extragalactic dark matter annihilation gamma-ray background. The color code is the same as for previous figures. We assume that dwarf spheroidals have no substructure boost. The fiducial model does not favour indirect searches with clusters. The inversion of predictions for Coma and Fornax between top and bottom panels accounts for source extension, as explained in the main text.

PDF of observing P(F) [all halos in pixel]: DM extragalactic vs astro

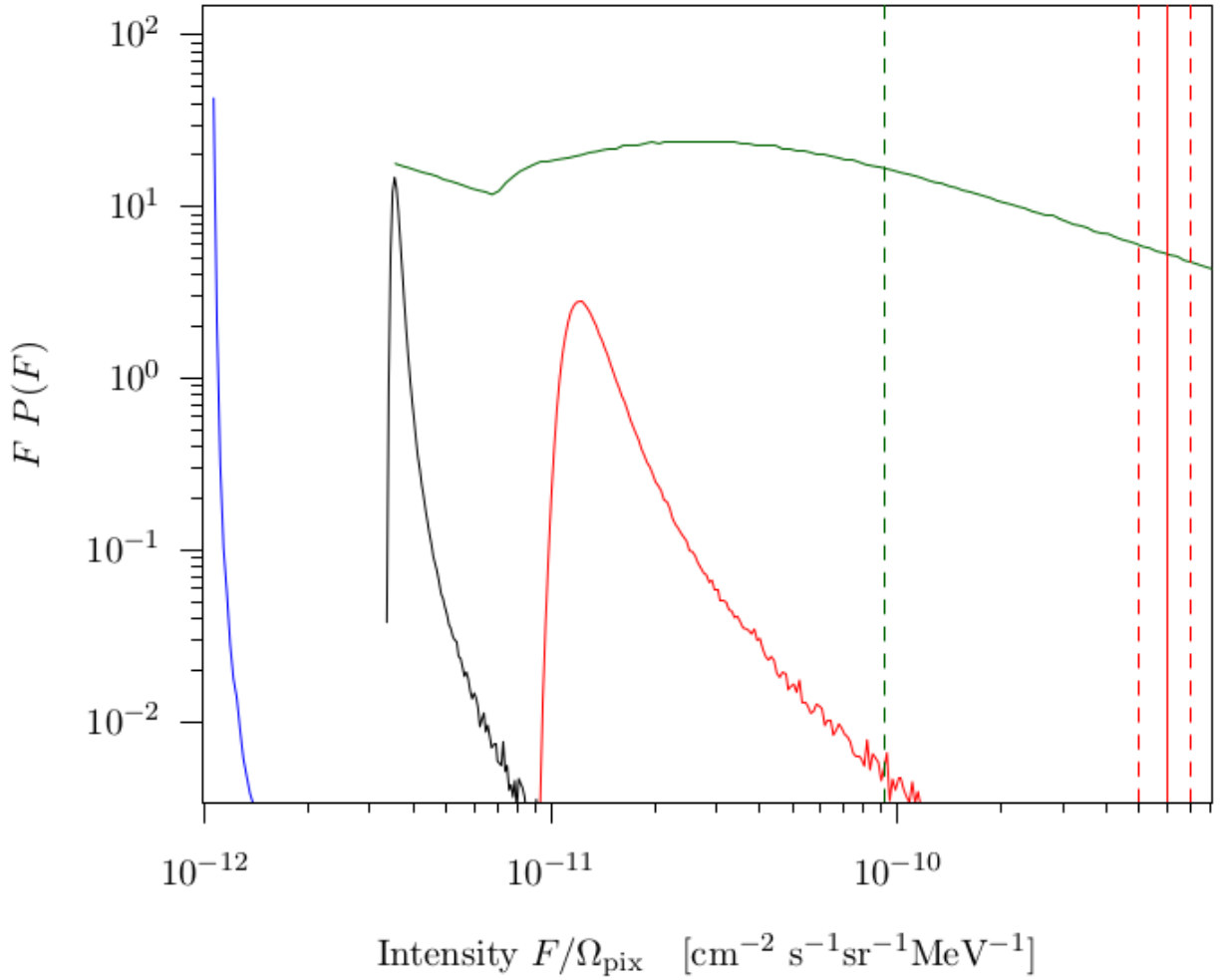

Figure 5. One-point function $P(F)$ for the three dark matter models (with boosts color-coded as previously), alongside the $P(F)$ of the diffuse contribution of blazars (green). The dashed red band represents the measurement of the unresolved EGB from the Fermi data at 1 GeV [66], while the dashed green line is the mean of the blazar PDF.

PDF of observing P(F) [all halos in pixel]: DM extragalactic vs astro

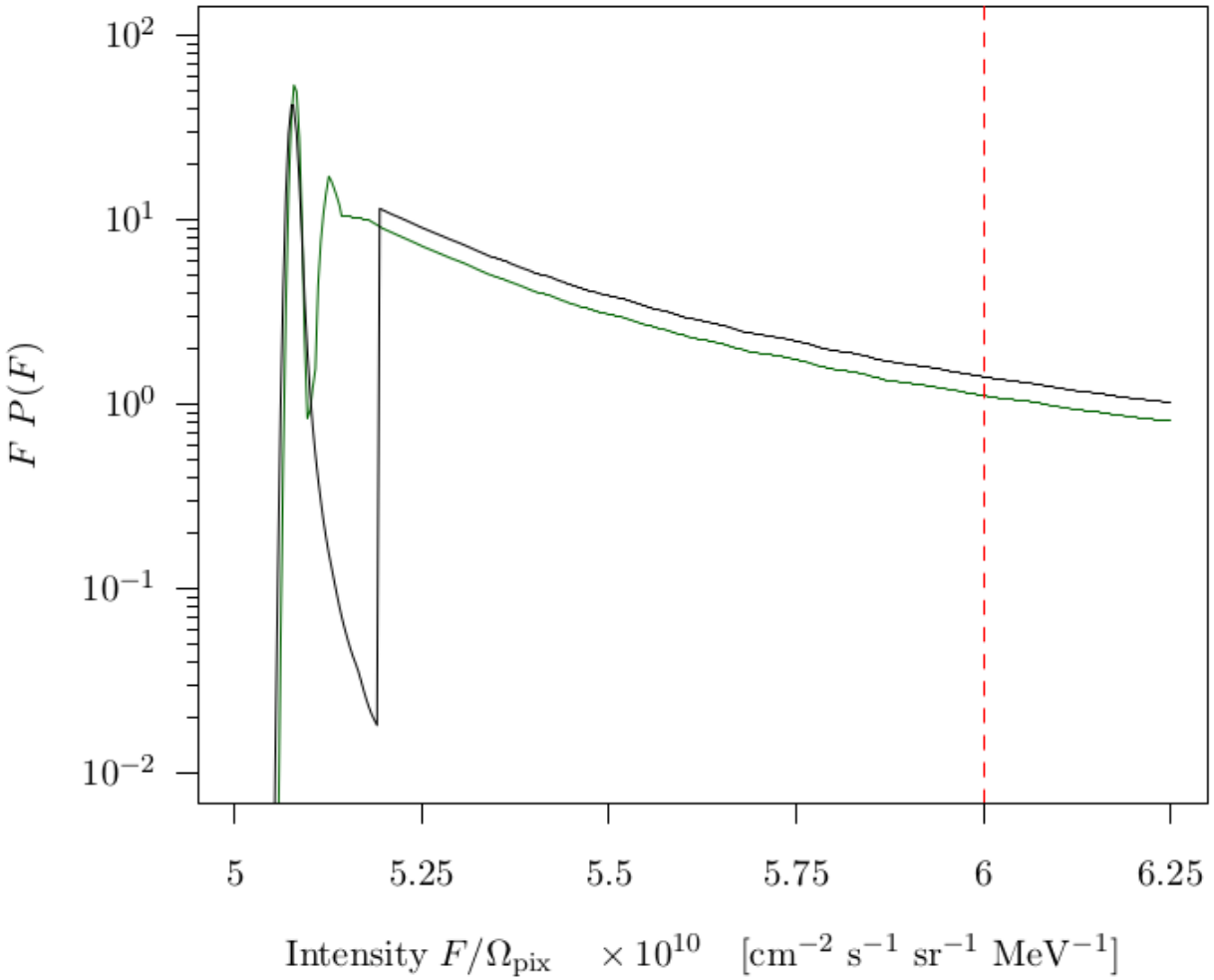

Figure 6. Predicted flux distribution $P_{\rm EGB}(F)$ of the extragalactic gamma-ray background, with (black) and without (green) a contribution from dark matter annihilations. The distributions have two peaks, based on whether or not a blazar is present in the associated pixel. The mean EGB derived from Fermi [66] is represented by the vertical line (red, dashed). A cross-section twice the canonical value was used to visually enhance the differences between these distributions.

PDF of observing P(C) [all counts in pixel]: statistical test

5.3 The photon count distribution $P(C)$

The observable given by Fermi is not the gamma-ray flux F, but the discrete number of photon counts per pixel C. Photon arrival may then be modelled as a Poisson rate with a mean determined by the differential gamma-ray flux and the exposure $\epsilon = (\text{time}) \times (\text{detector area}) \times (\text{photon energy})$. For a five-year Fermi mission, correcting for the field of view, we have an exposure of $\epsilon \approx 2.83 \times 10^{14}$ cm^2 s MeV sr pixel^{-1}. Marginalising over the uncertain flux distribution then gives

$$P(C) = \int P_{\mathrm{EGB}}(F) \mathcal{P}\left(C|\epsilon F\right) dF. \tag{5.8}$$

This Poisson arrival uncertainty substantially smooths away the differences between the null and alternate flux models, as evidenced by figure 7. However, the percent-level shift between the low-flux peaks due to the dark matter distribution's skewness survives, since a percent difference with $C \sim \mathcal{O}(100)$ is still a few photons. There is also a larger, opposite shift in the point-source-driven high-flux tail due to our imposed value of the distribution's mean.

We can define, given our number of pixels N_{pix}, the test statistic [25]

$$\chi^2 = \sum_C \left(\frac{N_{\mathrm{pix}}[P_{\mathrm{Null}}(C) - P_{\mathrm{Alt}}(C)]}{\sqrt{N_{\mathrm{pix}} P_{\mathrm{Null}}(C)}} \right)^2. \tag{5.9}$$

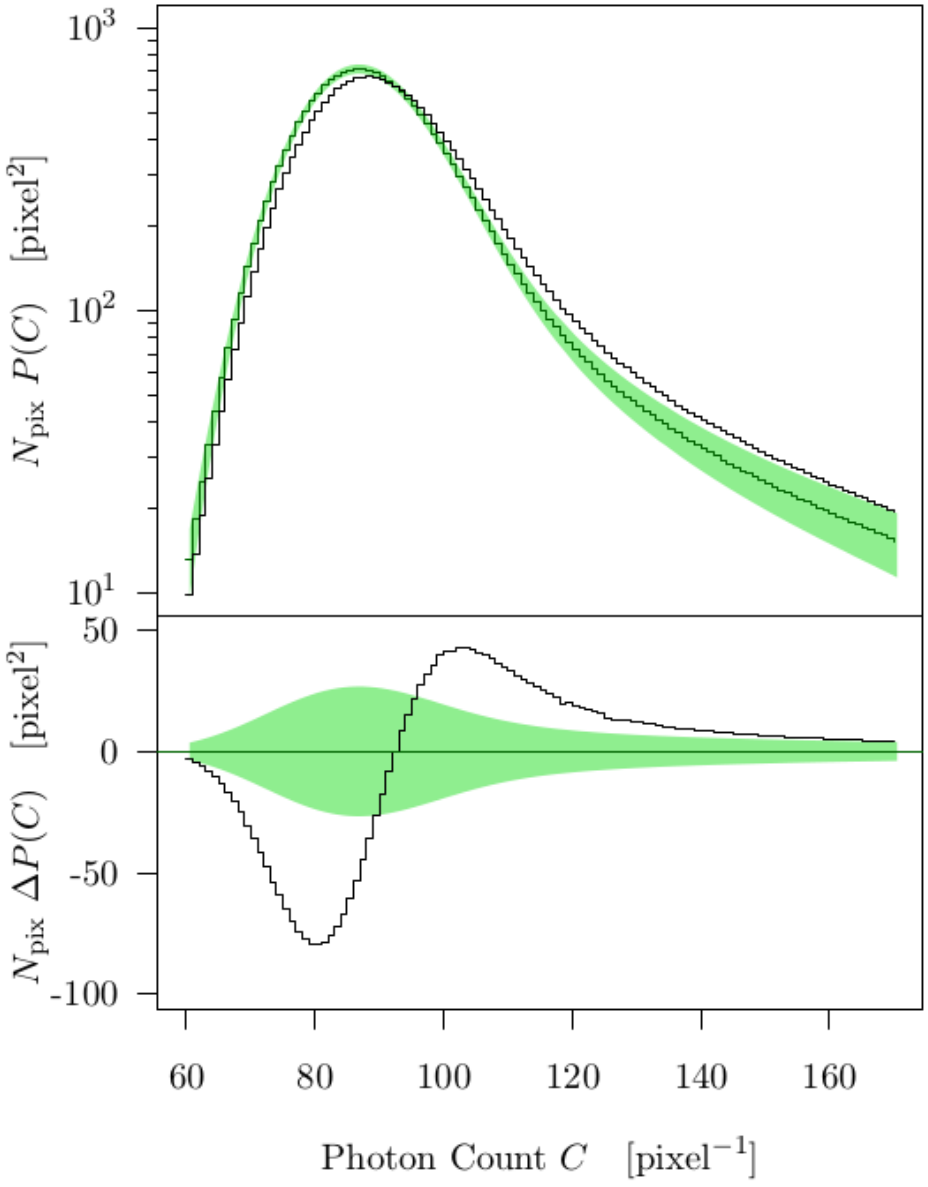

Figure 7. Predicted count distributions of EBG photons with (black) and without (green) a dark matter component. The green bands represent the Poisson errors $\sigma \propto \sqrt{N\,P(C)}$ on the dark-matter-free model. The lower panel shows difference between the two models. A cross-section twice the canonical value was used to visually enhance the differences between these distributions.

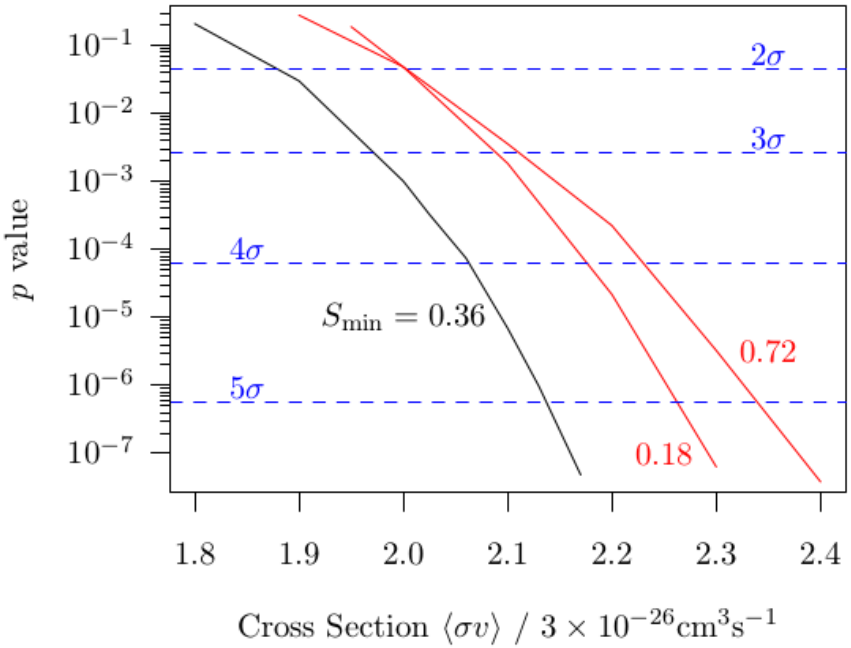

Figure 8. Predicted statistical significance of a (hypothetical) one-point-function-only detection of a dark matter annihilation signal above perfectly characterised astrophysical backgrounds, as a function of the dark matter cross-section. Curves are labelled by the flux $S_{\rm min}$ down to which the blazar distribution is extrapolated (see table 3). Horizontal lines (blue, dashed) represent some common choices of confidence level. Including the energy-dependence of the flux distributions would improve these results, at the cost of a greater dependence on the annihilation spectrum.

they remain smaller than a factor of three. We then compute, without requiring any additional physical assumptions, the flux distribution per pixel $P(F)$, which has the characteristic form of an isotropic diffuse Gaussian matched at high flux to the point-source distribution with a power-law slope of -2.5. This distribution is non-Gaussian and asymmetric; however the most likely flux and the mean flux are comparable at the percent-level in all but the optimistic boost model, salvaging previous 'mean intensity' constraints on the dark matter properties from this potential systematic effect.

The fluxes predicted for our fiducial model lie just within the reach of the Fermi-LAT, and should be observable by the tenth year of the mission. We also showed that the dis-